The Astrophysical Journal Letters, 717:L118–L121, 2010 July 10 doi:10.1088/2041-8205/717/2/L118

GeV BREAKS IN BLAZARS AS A RESULT OF GAMMA-RAY ABSORPTION WITHIN THE BROAD-LINE REGION

Juri Poutanen[1] and Boris Stern[1,2,3]
[1] Astronomy Division, Department of Physics, P.O. Box 3000, 90014 University of Oulu, Oulu, Finland; juri.poutanen@oulu.fi
[2] Institute for Nuclear Research, Russian Academy of Sciences, Prospekt 60-letiya Oktyabrya 7a, Moscow 117312, Russia; boris.stern@gmail.com
[3] Astro Space Center, Lebedev Physical Institute, Profsoyuznaya 84/32, Moscow 117997, Russia
Received 2010 May 20; accepted 2010 June 8; published 2010 June 21

ABSTRACT

Spectra of the brightest blazars detected by the *Fermi Gamma-ray Space Telescope* Large Area Telescope cannot be described by a simple power-law model. A much better description is obtained with a broken power law, with the break energies of a few GeV. We show here that the sharpness and the position of the breaks can be well reproduced by absorption of γ-rays via photon–photon pair production on He II Lyman recombination continuum and lines. This implies that the blazar zone lies inside the region of the highest ionization of the broad-line region (BLR) within a light-year from a super-massive black hole. The observations of γ-ray spectral breaks open a way of studying the BLR photon field in the extreme-UV/soft X-rays, which are otherwise hidden from our view.

Key words: BL Lacertae objects: general – galaxies: active – galaxies: jets – gamma rays: general – radiation mechanisms: non-thermal

Online-only material: color figures

1. INTRODUCTION

The *Fermi Gamma-ray Space Telescope* has detected more than a hundred blazars in the 100 MeV–100 GeV range (Abdo et al. 2009b) and allowed their detailed spectral studies with unprecedented accuracy. A surprising result is that the spectra of high-luminosity sources, flat-spectra radio quasars (FSRQs) and low-energy synchrotron-peaked BL Lac objects, are much better described by a broken power law than by a simple power law or any smoothly curved models (Abdo et al. 2009a, 2010). The break energies, mostly lying in the 2–10 GeV range (as measured in the object frame), seem to be too small to be produced by the γ-ray absorption due to photon–photon pair production in the broad-line region (BLR), as the strongest BLR line, Lyα, absorbs γ-rays starting from only 25.6 GeV. The observed spectral breaks are also too sharp, and the change in the spectral indices is too large to be associated with the cooling or the Klein–Nishina effects (Ghisellini & Tavecchio 2009).

Calculations of the γ-ray absorption within the BLR are usually limited to the contribution from lines in the observed optical band (e.g., Liu & Bai 2006; Reimer 2007) with a few exceptions (Tavecchio & Mazin 2009). Theoretical models, however, predict strong helium UV lines as well as metal lines in the soft X-rays (see, e.g., Krolik 1999), because a typical quasar spectrum has a power-law tail extending to the X-ray band (Laor et al. 1997). In addition to the lines, there are strong recombination continua of hydrogen and He II at 13.6 and 54.4 eV, respectively. These sharp, line-like features cause jumps in the γ-ray opacity at $\sim$19.2 and 4.8 GeV. We propose here that the observed spectral breaks in blazars are produced by absorption on photons of these recombination continua.

2. GAMMA-RAY ABSORPTION WITHIN THE BROAD-LINE REGION

2.1. Emission From the Broad-line Region

The BLR around quasars is known to emit a number of strong lines associated with very different ionization stages. Reverberation mapping of Seyfert galaxies and quasars using the C IV λ1549 line showed that the size of the BLR scales with the luminosity as (Kaspi et al. 2007)

$$R_{\mathrm{C\,IV},18} \approx 0.4 L_{47}^{1/2}. \quad (1)$$

The estimated BLR size is, however, 2–3 times larger for the Balmer lines and 3 times smaller for high-ionization He II λ1640 and N V λ1240 lines (Korista et al. 1995; Peterson & Wandel 1999). This argues in favor of strong radial ionization stratification of the BLR spanning over an order of magnitude in radius. The BLR spectrum is thus very much dependent on the distance from the central ionizing source.

Using spectral synthesis code XSTAR (version 2.2, Kallman & Bautista 2001), we generated a grid of photoionization models of BLR clouds assumed to be simple slabs of constant gas density and a clear view to the ionizing source. For simplicity, we fix the cloud column density at $N_{\mathrm{H}} = 10^{23}$ cm^{-2} and vary the ionization parameter $\xi = L/(r^2 n_{\mathrm{H}})$ from $10^{0.5}$ to $10^{2.5}$. We assume a gradual change of the cloud density as a function of distance from the central source, $n_{\mathrm{H}} \propto r^{-1}$. Taking $n_{\mathrm{H}} = 10^{11.5}$ cm^{-3} at the inner edge of the BLR, the distances r to the ionizing source are between 0.03 ($\log \xi = 2.5$) and 1 pc ($\log \xi = 0.5$) for a quasar luminosity $L = 10^{47}$ erg s^{-1}. This BLR model is broadly consistent with the constraints from reverberation mapping (Kaspi & Netzer 1999). It is, of course, still an oversimplification, but this is enough to show the impact of BLR on propagation of the GeV photons.

The quasar spectrum is taken as a sum of the standard multicolor accretion disk plus a power law of total luminosity 10% and extending to 100 keV (Laor et al. 1997). The resulting BLR spectra are shown in Figure 1(a). Their absolute normalization depends on the covering fraction of the BLR clouds. If it does not vary dramatically over distance, the radiation field at a given radius is dominated by the locally produced photons corresponding to a specific ionization parameter. As our aim is not the study of the BLR emission, but its effect on the high-energy photon propagation, we smooth the spectrum to show the most significant features (see Table 1). In the high-ionization zone at

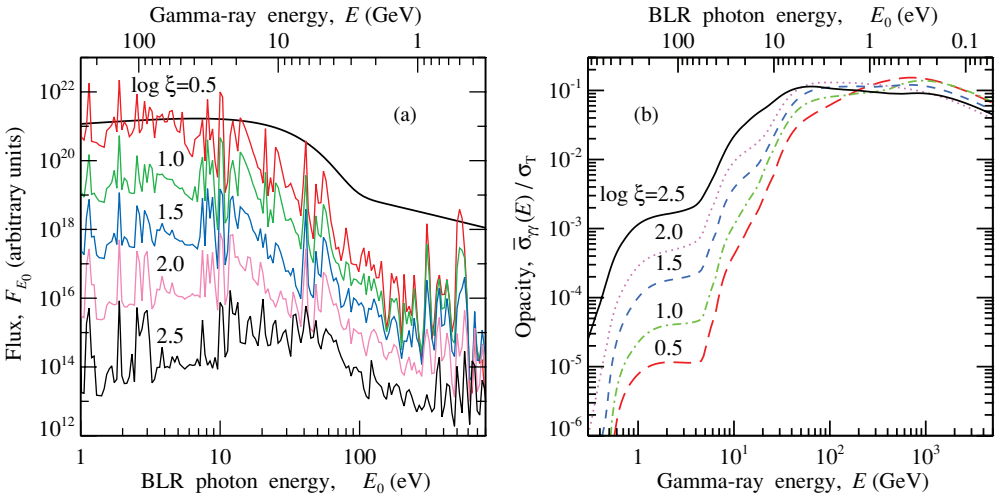

Figure 1. (a) Spectrum of the broad emission line region. The spectra for various ionization parameters ξ computed using a photoionization code XSTAR version 2.2 (Kallman & Bautista 2001) are averaged on a logarithmic energy grid with the 5% spectral resolution to show the most significant features dominating the total flux. The incident typical quasar spectrum (Laor et al. 1997) shown by a smooth curve consists of a multicolor disk with the maximum temperature 10^5 K and a power-law tail of photon index $\Gamma = 2$ extending to 100 keV with 10% of the total luminosity. (b) Average cross section (in units of Thomson cross section) for γ-rays due to photon–photon pair production on the broad-line region (BLR) spectra shown in panel (a). Opacity produced by the disk radiation, direct or scattered outside the BLR clouds (see, e.g., Blandford & Levinson 1995), is neglected here. Jumps in opacity are clearly seen at energies corresponding to the strongest lines and recombination continua. The 0.3–0.5 GeV jump for large ξ is produced by O VIII $\lambda\lambda$16–19 lines, the jump at low ξ is due to the O VII λ22 line complex (see Table 1). The jump at $\sim$5 GeV visible at all ionizations is due to the He II recombination continuum and Ly lines at 40–60 eV. The 20–30 GeV jump seen at low ξ is produced by H I Ly lines and continuum and the C IV λ1549 line.

(A color version of this figure is available in the online journal.)

Table 1
BLR Strongest Lines and Recombination Continua Causing Jumps in the γ-ray Opacity

Feature	λ_{BLR}[a] (Å)	E_{BLR}[b] (eV)	E_γ[c] (GeV)
Low-ionization lines			
O VII (blend)	22	560	0.47
C V (blend)	40.5	305	0.86
Low-ionization H I 10 eV complex			
Ly continuum	911	13.6	19.2
Lyα	1215	10.2	25.6
C IV	1549	8.0	32.6
Low-ionization He I 20 eV complex			
He I rec. continuum	504.2	24.6	10.6
He I	584.3	21.2	12.3
High-ionization lines			
O VIII	16.01	774	0.34
O VIII	18.97	653	0.40
C VI	33.74	367	0.71
He II 50 eV complex			
He II Ly continuum	227.8	54.4	4.8
Fe XV	284.2	43.6	
Si XI	303.3	40.9	
He II Lyα	303.8	40.8	6.4

Notes.
[a] Wavelength of the spectral feature.
[b] Energy of the spectral feature $E_{BLR}(\mathrm{eV}) \approx 12393/\lambda_{BLR}(\text{Å})$.
[c] Energy of the jump in the γ-ray opacity $E_\gamma(\mathrm{GeV}) \approx 261/E_{BLR}$ (eV) $\approx \lambda_{BLR}(\text{Å})/47.5$.

small distances to the central source, He II Ly lines and recombination continuum at 40–60 eV are relatively strong. There are also significant soft X-ray lines of O VIII and C VI, which are important for estimation of the $\sim$500 MeV photon propagation. In the low-ionization zone at larger distances, hydrogen Ly lines and recombination continuum dominate the photon flux with the additional strong lines from C IV, C V, He I, He II, as well as helium recombination continua.

2.2. Absorption of GeV Photons

Photons produced in the BLR constitute the target for the GeV photons propagating through them. If the background isotropic photons have strong line-like features peaking at energy E_0, the photon–photon pair production cross section $\sigma_{\gamma\gamma}(s)$ for a photon of energy E is the function of the product of two energies $s = EE_0/(m_ec^2)^2$ (see, e.g., Gould & Schréder 1967; Zdziarski 1988). It has a threshold $s = 1$, rapidly grows to the maximum of about 20% of the Thomson cross section σ_T at $s \approx 3$, and then slowly decreases. The optical depth for a photon of energy E through the region of size R filled with photons of column density N_{ph} is $\tau_{\gamma\gamma}(E, E_0) = \tau_T\sigma_{\gamma\gamma}(s)/\sigma_T$, where

$$\tau_T = N_{ph}\sigma_T = \frac{L\sigma_T}{4\pi RcE_0} = 110\frac{L_{45}}{R_{18}}\frac{10\ \mathrm{eV}}{E_0}, \qquad (2)$$

and L is the line luminosity (we defined $Q = 10^x Q_x$ in cgs units). Equation (2) implies that it is not the luminosity, but its ratio to the typical size (i.e., compactness) that determines a role of a specific line in absorption of the γ-rays. Because of the luminosity dependence of the BLR size, the opacity also depends on it as

$$\tau_T \propto L^{1/2}. \qquad (3)$$

This provides a simple explanation of why the GeV breaks are observed only in the brightest blazars.

The spectrum transmitted through the region is attenuated as $\propto \exp(-\tau_{\gamma\gamma}(E, E_0))$. If the incident spectrum is a power law, a break appears above the threshold energy $(m_ec^2)^2/E_0$, where the spectral index changes by

$$\Delta\Gamma = -\frac{d\ln\exp(-\tau_{\gamma\gamma}(E, E_0))}{d\ln E} \approx \max\frac{\sigma_{\gamma\gamma}(s)}{\ln s} \approx \frac{\tau_T}{4}. \qquad (4)$$

The efficiency of γ-ray absorption within a BLR depends on the photon distribution, with the averaged photon–photon pair

Table 2
Spectral Properties of Blazars

Object	z	Power Law	Broken Power Law				Power Law + Double Absorber			
		χ^2	Γ_1	Γ_2	$E_{\rm break}(1+z)$(GeV)	χ^2	Γ	$\tau_{\rm He}$	$\tau_{\rm H}$	χ^2
3C 454.3	0.859	117	2.36 ± 0.02	3.60 ± 0.22	4.5 ± 0.5	6.5	2.37 ± 0.02	6.1 ± 0.9	18.5^{+19}_{-7}	4.1
PKS 1502+106	1.839	55	2.15 ± 0.03	2.87 ± 0.16	7.8 ± 1.5	7.8	2.13 ± 0.03	1.6 ± 0.6	8.4 ± 1.6	6.3
3C 279	0.536	18	2.17 ± 0.07	2.56 ± 0.09	1.8 ± 0.6	4.6	2.28 ± 0.04	2.0 ± 1.1	4.5 ± 3.1	10.1
PKS 1510–08	0.36	13	2.43 ± 0.05	2.84 ± 0.27	3.1 ± 1.8	6.6	2.45 ± 0.04	2.7 ± 1.5	$2.7^{+8}_{-2.7}$	8.1
3C 273	0.158	10	2.82 ± 0.06	3.40 ± 0.42	$1.9^{+1.0}_{-1.9}$	6.1	2.87 ± 0.05	$3.6^{+6}_{-3.6}$	$0^{+\infty}_{-0}$	7.8
PKS 0454–234	1.003	50	2.04 ± 0.05	2.81 ± 0.17	5.3 ± 1.0	12.3	2.04 ± 0.04	3.0 ± 0.8	9.5 ± 2.7	13.7
PKS 2022–07	1.388	15	2.45 ± 0.05	3.02 ± 0.17	9.6 ± 4.3	11.6	2.48 ± 0.06	$0.8^{+0.9}_{-0.8}$	$2.9^{+4.3}_{-1.8}$	12.9
TXS 1520+319	1.487	11	2.49 ± 0.07	2.89 ± 0.24	4.7 ± 0.5	7.9	2.48 ± 0.74	1.7 ± 1.6	6.5^{+9}_{-5}	7.2
RGB J0920+446	2.19	21	1.99 ± 0.08	3.47 ± 0.4	19 ± 5	7.8	2.01 ± 0.07	$0^{+0.5}_{-0}$	7.6 ± 2.9	11.9

Note. The number of degrees of freedom is 12 for the power-law model and 10 for other models.

production cross section being

$$\overline{\sigma}_{\gamma\gamma}(E) = \frac{1}{N_{\rm ph}} \int \sigma_{\gamma\gamma}(s) N_{\rm ph}(E_0) dE_0. \quad (5)$$

Figure 1(b) presents the photon–photon pair production cross section averaged over the BLR spectra shown in Figure 1(a). If the ionization is high, the dominant photon source is the He II complex at 40–60 eV (see Table 1), which produces a break in opacity at 4–7 GeV. Above 10 GeV, the opacity is a rather smooth function of energy with additional absorption coming from He I, hydrogen Ly lines and recombination continuum, and C V λ2274. In the 0.3–0.7 GeV region, the opacity has another break due to high-ionization lines of O VII. Detection of this break requires $\tau_{\rm T} \gtrsim 300$, which certainly is enough to completely absorb the GeV radiation.

In the low-ionization environment, the strongest absorption is produced by hydrogen Ly lines and recombination continuum, forcing a break in opacity at about 20–30 GeV. At the same time, the break due to helium is also clearly visible at a few GeV. The breaks below 1 GeV would probably be impossible to detect due to low opacity at these energies. The opacity is nearly flat up to 1 TeV (Tavecchio & Mazin 2009) because of the contribution from additional lines: Mg II λ2800, Hα, and He I λ10832.

The breaks at 4–7 and 20–30 GeV are expected for a large range of ionization parameters. The total opacity in 5–50 GeV range can therefore be very roughly represented as a sum of opacities resulting from two "lines" at ionization energies of He II and H I, 54.4 and 13.6 eV, taken in different proportions. The opacity in these lines can be characterized by the optical depths $\tau_{\rm He}$ and $\tau_{\rm H}$, which reflect the column density of photons at respective energies via Equation (2). In this simple approximation, which we will call a double-absorber model, the breaks appear at 4.8 and 19.2 GeV.

3. BLAZARS OBSERVED BY *FERMI*

We analyze the data for several brightest FSRQs from the sample of 12 objects in Table 1 in Abdo et al. (2010) and choose the same 180 day interval for easier comparison. We cannot use the standard software distributed by the LAT team, because it does not contain the required spectral models. Instead, we wrote our own version and checked its performance by comparing its results for the simple broken power-law models with those obtained by Abdo et al. (2010) using the standard maximum likelihood analysis tool *gtlike*. We excluded three objects for which our simplified analysis is not adequate: 4C+38.41 and PKS 0528+134, because of severe source confusion, and PKS 1908–201, since it is close to the Galactic bulge and the background is high.

3.1. Data Analysis

We use class 3 (diffuse) photons and impose the cuts at zenith angle $<105^\circ$ and incident angle to the detector axis $<60^\circ$. The latter cut excludes counts with very low value of the detector response and restricts variation of the count weight by factor ∼2.7. We used `P6_V3_DIFFUSE` version of the response function. The background was measured in a circle with the radius 6°, separated from the object by ∼15° and avoiding local sources. We accumulate counts in the circle centered at the source location with the energy-dependent radius $r = \max\{10^\circ (E/100\ {\rm MeV})^{-0.7}, 0.^\circ 6\}$ (which corresponds to 95% containment).

At this stage, we are not interested in the absolute normalization of the spectrum, but only in its shape, therefore our strategy is to sample the response function at photon arrival times (rather than integrating it over time). As the energy resolution in the range of interest (1–30 GeV) is good enough, we can treat the response matrix as diagonal and just prescribe to each photon the weight inversely proportional to the effective area for the given energy and incident angle. We restrict the spectral fit to energies above 200 MeV. We use binned fitting as it provides us with a very simple and clear indicator of the fit quality, χ^2. For a few bins at high energies, where the number of photons is low, we use Poisson likelihood adding $-2 \log P(n, \mu)$ to χ^2 (here n is the number of counts in the bin and μ is the prediction of the model). The number of such bins is small and the meaning of χ^2 is not significantly affected. For the minimization we use the standard code MINUIT from the CERN library.

3.2. Spectral Fits

First, we fit the data with a simple power-law model. For five objects out of nine from our sample, the fits are acceptable ($\chi^2 < 18$ for 12 degrees of freedom). Next, we apply the broken power-law model with parameters Γ_1, Γ_2, $E_{\rm break}$ and free normalization (see Table 2). There is a good agreement with the results by Abdo et al. (2010), except for RGB J0920+446 (where the best-fit parameters given by Abdo et al. (2010) evidently do not match the spectrum of the object presented in the same paper) and for PKS 0454–234 (where our minimization routine probably found a different local minimum). The breaks are not statistically significant in PKS 1510–08, 3C 273, PKS 2022–07, and TXS 1520+319.

Finally, we have fitted the data with a power law and the double-absorber model taking optical depths $\tau_{\rm He}$ and $\tau_{\rm H}$,

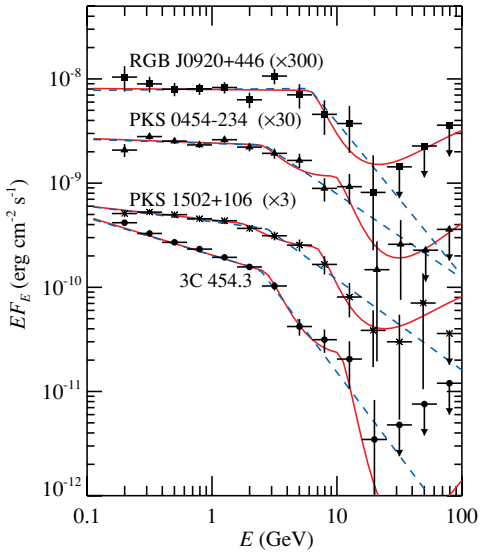

Figure 2. Spectral energy distribution of a few blazars as observed with *Fermi*/LAT. The best-fit broken power law and a power law with the double-absorber models are shown by the dashed and solid lines, respectively.

(A color version of this figure is available in the online journal.)

photon index Γ, and normalization as free parameters. The "lines" were redshifted by the appropriate $1 + z$ factor. The fits give statistically significant detections of absorption with a good χ^2 for 3C 454.3, PKS 1502+106, PKS 0454–234, and RGB J0920+446 (see Table 2 and Figure 2). Upper limits on absorption for PKS 1510–08, PKS 2022–07, and TXS 1520+319 are significantly smaller than the absorption optical depth for 3C 454.3. There are no significant constraints for 3C 273. The quality of the fits with the absorption model is about the same as with the broken power-law model with the same number of parameters. In fact, the absorption model is less flexible as the energy, where the power-law spectrum breaks, is fixed.

4. DISCUSSION AND SUMMARY

The GeV breaks observed in blazars are well described by γ-ray absorption via photon–photon pair production on He II and H I recombination continuum photons. In RGB J0920+446, the absorption is seen only at high energies with the break energy $E_{\rm break}$ corresponding to the pair-production threshold on hydrogen recombination photons, while in other cases the break is close to the threshold for the absorption on He II recombination continuum. The exact position of the break depends on the ionization parameter that determines the contribution of metals and affects the position of the centroid of the 50 eV complex. If $\tau_{\rm He}$ is small, then the break shifts to 19 GeV as observed in RGB J0920+446.

A rather large ratio of the fitted optical depths $\tau_{\rm He}/\tau_{\rm H} \sim 1/4$ implies that the γ-ray emitting region has to lie within the high-ionization zone of the BLR with $\log \xi > 2$. For the brightest γ-ray object in our sample, 3C 454.3, with its accretion luminosity of about 10^{47} erg s^{-1} (Smith et al. 1988), the high-ionization zone should be within about 0.1 pc. This corresponds to about 10^3 Schwarzschild radii for an $\sim 10^9\ M_\odot$ central black hole (Bonnoli et al. 2010). At such a distance, the luminosity in the 50 eV complex can be as small as $\sim 10^{44}$ erg s^{-1}, a per mille of the accretion luminosity, to provide the necessary opacity with $\tau_{\rm He} \sim 6$ (see Equation (2)).

The opacity measured above 20 GeV and the Lyα luminosity of 10^{45} erg s^{-1} observed in 3C 454.3 (Wills et al. 1995) allow us to estimate the Lyα emission zone size. Taking the recombination continuum luminosity equal to that of Lyα and using Equation (2) we get $R_{\rm Ly\alpha} = 2 \pm 1$ pc, which indicates that absorption at these energies happens at a larger distance than absorption by He II photons.

The constraints obtained on the γ-ray emission site imply that the jet is already accelerated to a relativistic velocity within a thousand gravitational radii. It also strongly constrains the mechanisms for γ-ray production. The possible sources of soft photons for Comptonization in the jet are the accretion disk (Dermer & Schlickeiser 1993) and the BLR (Sikora et al. 1994). As a source of photons, the dust emission at 10 pc scale (Błażejowski et al. 2000; Sikora et al. 2008) cannot be important.

Let us also remark that the GeV photons absorbed in the BLR produce electron–positron pairs which, spiraling in the magnetic field, radiate away their energy isotropically. This emission cannot compete with the beamed emission from the jet, but can contribute to the high-energy emission of radio galaxies observed at large angles to the jet axis (see, e.g., Roustazadeh Sh. & Boettcher 2010).

Our interpretation of the GeV breaks implies that additional breaks (depressions) at 0.3–0.7 GeV produced by the soft X-ray lines within the high-ionization zone should be seen, once the photon statistics is high enough. The γ-ray spectroscopy can be used as a powerful tool for studying the extreme-UV and soft X-ray emission in the quasars' vicinity, which is otherwise hidden from us by interstellar absorption.

This research was supported by the Academy of Finland grants 127512 and 133179 and the Väisälä foundation. The research made use of public data obtained from the *Fermi* Science Support Center. We thank Markus Boettcher, Evgeny Derishev, Julian Krolik, Amir Levinson, Fabricio Tavecchio, and Dmitry Yakovlev for useful comments and Tim Kallman for his help with XSTAR.

REFERENCES

Abdo, A. A., et al. 2009a, ApJ, 699, 817
Abdo, A. A., et al. 2009b, ApJ, 700, 597
Abdo, A. A., et al. 2010, ApJ, 710, 1271
Blandford, R. D., & Levinson, A. 1995, ApJ, 441, 79
Błażejowski, M., Sikora, M., Moderski, R., & Madejski, G. M. 2000, ApJ, 545, 107
Bonnoli, G., Ghisellini, G., Foschini, L., Tavecchio, F., & Ghirlanda, G. 2010, MNRAS, submitted (arXiv:1003.3476)
Dermer, C. D., & Schlickeiser, R. 1993, ApJ, 416, 458
Ghisellini, G., & Tavecchio, F. 2009, MNRAS, 397, 985
Gould, R. J., & Schréder, G. P. 1967, Phys. Rev., 155, 1404
Kallman, T., & Bautista, M. 2001, ApJS, 133, 221
Kaspi, S., Brandt, W. N., Maoz, D., Netzer, H., Schneider, D. P., & Shemmer, O. 2007, ApJ, 659, 997
Kaspi, S., & Netzer, H. 1999, ApJ, 524, 71
Korista, K. T., et al. 1995, ApJS, 97, 285
Krolik, J. H. 1999, Active Galactic Nuclei: From the Central Black Hole to the Galactic Environment (Princeton, N J: Princeton Univ. Press)
Laor, A., Fiore, F., Elvis, M., Wilkes, B. J., & McDowell, J. C. 1997, ApJ, 477, 93
Liu, H. T., & Bai, J. M. 2006, ApJ, 653, 1089
Peterson, B. M., & Wandel, A. 1999, ApJ, 521, L95
Reimer, A. 2007, ApJ, 665, 1023
Roustazadeh Sh., P., & Boettcher, M. 2010, ApJ, in press (arXiv:1005.2379)
Sikora, M., Begelman, M. C., & Rees, M. J. 1994, ApJ, 421, 153
Sikora, M., Moderski, R., & Madejski, G. M. 2008, ApJ, 675, 71
Smith, P. S., Elston, R., Berriman, G., Allen, R. G., & Balonek, T. J. 1988, ApJ, 326, L39
Tavecchio, F., & Mazin, D. 2009, MNRAS, 392, L40
Wills, B. J., et al. 1995, ApJ, 447, 139
Zdziarski, A. A. 1988, ApJ, 335, 786